Journal of Electron Microscopy **51(Supplement)**: S279–S287 (2002)

Full-length paper

Quantification of lattice images: the contribution from diffuse scattering

Chris B. Boothroyd

Department of Materials Science and Metallurgy, University of Cambridge, Pembroke Street, Cambridge, CB2 3QZ, UK
E-mail: cbb4@cam.ac.uk

Abstract At present, quantitative comparisons of experimental and simulated high-resolution images show that the contrast in experimental images is usually much less than is predicted by simulations, typically by a factor of around three. Investigations of this contrast discrepancy in images of amorphous carbon have shown that the contrast in experimental images is lower than in simulations by the same factor for a wide range of spatial frequencies, suggesting the possibility that the contrast loss is due to the addition of a constant background to the experimental images. The source of this constant background is investigated using convergent-beam diffraction patterns as a function of thickness and lattice images from an [001]-oriented crystal of GaAs. The diffuse background is measured in the convergent-beam patterns and found to contribute about 33% of the total intensity at 25 nm thickness. However, at this thickness the experimental lattice image contrast is only about half that of a simulated lattice image. Thus, although the measured diffuse scattering produces a significant contrast reduction in lattice images, the diffuse scattering from phonons and amorphous carbon is not sufficient to explain why lattice images have such low contrast.

Keywords convergent-beam electron diffraction (CBED), quantitative HREM, phonon scattering, diffuse scattering, lattice images, energy filtering

Received 13 November 2000, accepted 5 November 2001

Introduction

It has been recognized for a while now that high-resolution electron microscope image simulations provide a good *qualitative* match to experimental lattice images, but *quantitatively* the lattice fringe contrast in experimental images is lower than that in simulated images, typically by a factor of about three [1–3]. Possible causes of this discrepancy have been discussed by Boothroyd [4]. Firstly, the intensity and pattern of convergent-beam diffraction patterns have been found to match simulations quantitatively [5–7], although such measurements have been performed on relatively thick specimens, e.g. 250 nm thick. This suggests that the dynamical scattering process is modelled well by image simulations. Part of the process of comparing experimental and simulated convergent-beam patterns involves subtracting a diffuse background from each diffraction disc, since such diffuse scattering is not modelled by most simulation programs. Secondly, bright-field and dark-field thickness fringes have been compared quantitatively by many authors and absorption parameters deduced [8–10]. Such comparisons are essentially measuring the intensity of the 000 and diffracted beams as a function of crystal thickness and show that both bright-field and dark-field thickness fringes match simulations quantitatively over a wide range of thicknesses to better than 5%, although frequently the match is worst for the lowest thicknesses in dark-field. Again, this suggests that the calculation of the beam intensities is correct for a wide range of specimen thicknesses.

Boothroyd [11] measured the contrast of amorphous carbon films as a function of spatial frequency and found that the contrast in experimental images was low by a factor of three for frequencies from 0.5 to 5 nm^{-1}. This suggests that the lack of contrast is due to the addition of a constant background intensity to high-resolution images. If the images were being blurred, e.g. by specimen vibration, then the high frequencies would be reduced more than the low frequencies. The most likely causes for a constant background intensity in lattice

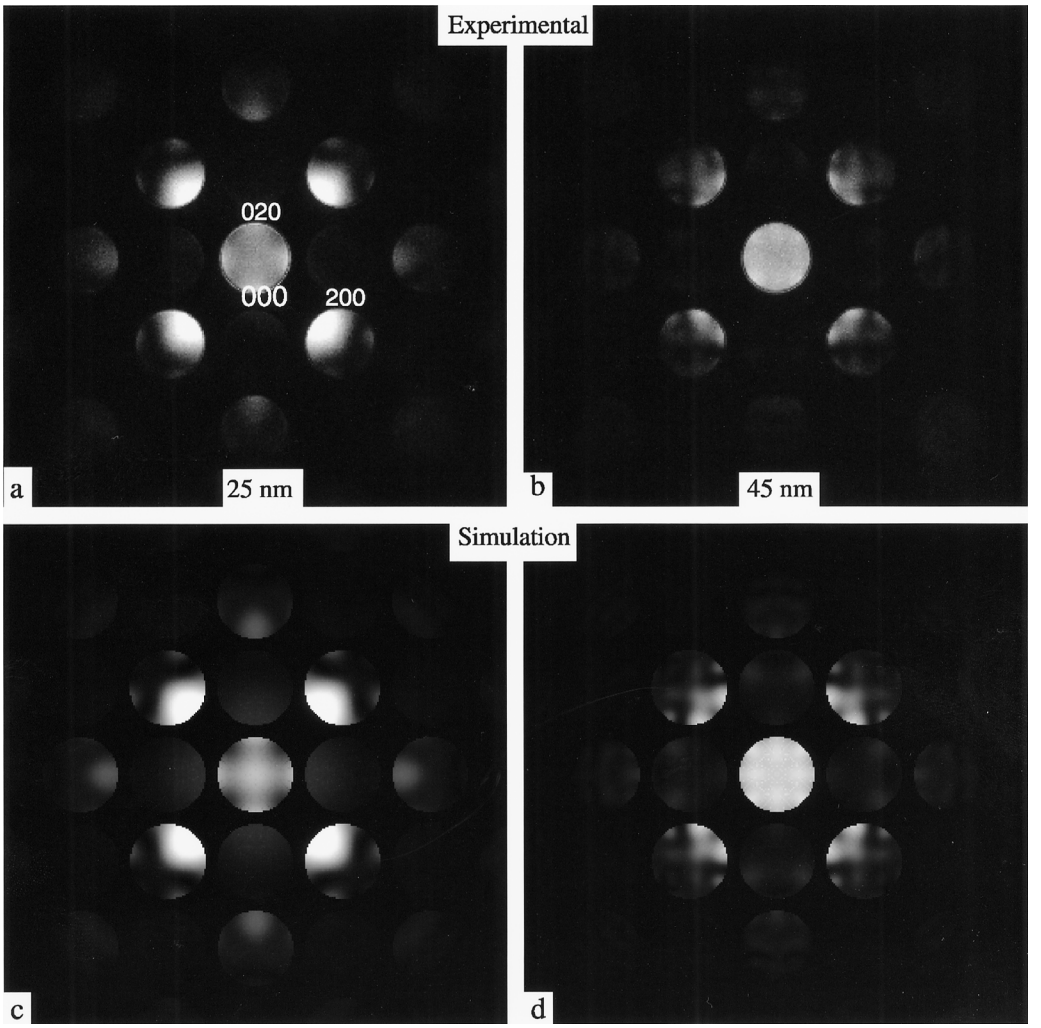

Fig. 1 (a, b) Experimental and (c, d) simulated convergent-beam patterns from [001] GaAs displayed on the same scale with black = 0 and white = 0.22 for specimen thicknesses of (a, c) 45 nm and (b, d) 85 nm.

images are amorphous layers and phonon scattering. Both of these are consistent with the presence of a diffuse background in convergent-beam patterns. Thus, the aim of this paper is to measure the diffuse background contribution to lattice images by collecting energy-filtered convergent-beam patterns as a function of specimen thickness from a 90° cleaved wedge of GaAs. This can be done by measuring the diffuse intensity between the diffracted discs and extrapolating under the diffraction discs. The measured diffuse intensities can then be correlated with the lattice fringe contrast from energy filtered lattice images collected from the same material. Although cleaved GaAs has a small unit cell making quantitative pattern matching of lattice images ambiguous, it has the advantage of a known relation between distance from the specimen edge and specimen thickness combined with a lack of amorphous damage layers.

For this work, it is important to understand the causes of diffuse scattering in experimental images and how this is allowed for in image simulations. For a cleaved specimen there will be no amorphous damage layer, so scattering from amorphous material is confined to carbon contamination. The characteristic diffuse scattering of amorphous carbon will have the effect of reducing the intensity of all GaAs diffracted beams in proportion and adding this intensity to the gaps between the beams. To a good approximation, we can assume that the scattering is uniform under the diffracted beams.

Phonon (thermal diffuse) scattering is caused by atoms being vibrated by thermal motion. Over time, the effect is to smear out the atoms. For high-energy electrons, the time taken for each electron to pass through the crystal is much smaller than the vibration period of the atoms, but the interval between electrons is much longer than the vibration period. Thus, to one electron the atoms appear frozen in one configuration but the next electron sees a different configuration of frozen atoms. There are three ways of dealing with phonon scattering in image simulations, the Debye–Waller factor, the Einstein phonon model, and the Debye phonon model.

The Debye–Waller factor smears out the atoms by convo-

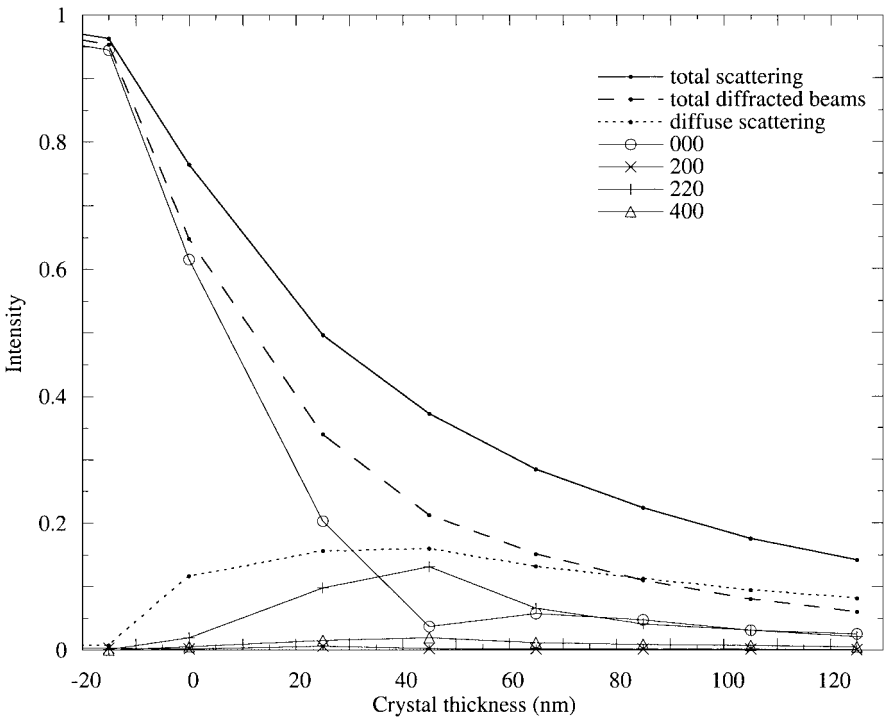

Fig. 2 Beam intensities measured from a series of experimental energy-filtered convergent-beam patterns like those in Fig. 1, as a function of crystal thickness. The convergent-beam patterns were taken by moving the beam in steps of 10 nm across the specimen resulting in thickness steps of 20 nm between each pattern. All intensities are normalized so that the incident intensity is 1. 'Total scattering' is the sum of all intensity in the convergent-beam pattern, 'diffuse scattering' is the sum of all the diffuse scattering between the beams plus that estimated to lie under the beams, and 'total diffracted' is the sum of all the diffracted beam intensities after the diffuse scattering has been removed from them. Also plotted are the intensities of a selection of beams, after subtraction of the diffuse intensity. The 200, 220, and 400 intensities are the sum of all 4 equivalent beams. Negative thicknesses correspond to distances away from the edge of the crystalline part of the specimen into the contamination layer, with –20 nm corresponding to a distance of 10 nm.

luting the atomic potential with a Gaussian representing the average thermal vibration amplitude. Thus, all the atoms in the calculation remain centred on their equilibrium positions but become a little broader. The Debye–Waller factor thus reduces the scattering to the higher order beams. Given that no diffuse intensity is produced between the diffracted beams and no electrons are lost in the calculation, the net effect is to increase the electrons in the 000 and low-order beams. In this respect, the Debye–Waller factor models experimental beam intensities well, but it does not model the diffuse intensity between the beams. Electrons that would be scattered diffusely remain in the low-order beams. To make simulations match experiment, the absorption parameters have to be adjusted for the objective aperture used to allow for the effect on the image of the diffuse scattering between the beams.

In the Einstein model, atoms are considered to be vibrating independently of each other. In an image simulation, no Debye–Waller factor is used, but instead the atoms are displaced randomly from their equilibrium sites. The calculation must be repeated for many different configurations of random displacements and averaged. 'Frozen phonon' calculations based on this model (e.g. Loane *et al*. [12]) model both the reduction in high-order diffracted beam intensities and the diffuse background and in addition model Kikuchi lines, caused by the diffuse scattering being diffracted by the crystal. The randomly displaced atoms in this model give rise to a nearly uniform diffuse background that is not peaked at the diffraction spots.

In reality, thermal vibrations are highly coupled between atoms and are better modelled as displacement waves in the lattice as in the Debye model. If the phonon spectrum is known, then the Einstein model above can be improved by averaging over atoms displaced by many phonons. The result is that the diffuse scattering is peaked at the diffraction maxima in agreement with observations [13–15]. The coupled vibrations of the Debye model and the random vibrations of the Einstein model predict the same intensity distribution in a lattice image, even though they predict different diffraction patterns [15]. Thus, for simulating lattice images, the Einstein model is sufficient. However, when measuring diffraction peak intensities, the concentration of diffuse scattering around diffraction maxima will lead to an underestimate of the diffuse scattering contribution to the diffraction spots and, thus, an overestimate of the diffraction contribution.

In this investigation, the Debye–Waller factor is used to model phonon scattering as in most conventional lattice image simulations. The amount of diffuse scattering between the GaAs diffracted beams is measured from convergent-beam

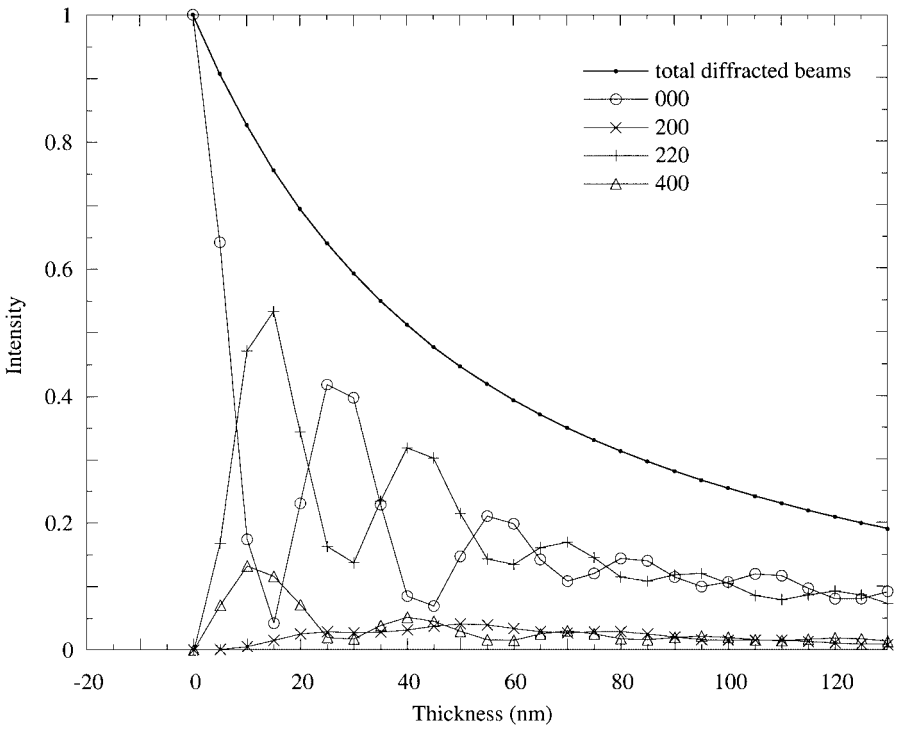

Fig. 3 Beam intensities measured from a series of simulated energy-filtered convergent-beam patterns and plotted in a similar way to Fig. 2. The Bloch wave simulations used a Debye–Waller factor to account for phonon scattering and, thus, do not have any diffuse scattering between the beams.

patterns by assuming phonon scattering is not peaked at the diffraction maxima, in effect assuming the Einstein model. This will give a lower limit to the actual amount of diffuse scattering. An estimate of the effect this diffuse scattering has on lattice image simulations can then be made by assuming that the diffuse scattering produces no lattice image contrast, but just adds a uniform background to the lattice images.

Methods

In this experiment, a Philips CM300 FEG electron microscope operated at 297 kV was used to record convergent-beam patterns and lattice images from a GaAs cleaved wedge specimen oriented with the beam along [001]. The 90° wedge angle of this specimen means that the crystal thickness can be determined easily as twice the distance from the edge of the specimen. The images were energy filtered using a Gatan imaging filter with an energy selecting slit width of 10 eV. This slit is narrow enough to exclude all the plasmon scattering, but will naturally not exclude phonon scattering. For the convergent-beam patterns, a Digital Micrograph script was used to control the beam position and acquire the diffraction patterns. The lattice images were collected from a fresh area of the specimen adjacent to the area the convergent-beam patterns were taken from. It should be emphasized that all lattice images and diffraction patterns were energy filtered, so there is no loss of contrast due to plasmon and core loss inelastic scattering.

Results

Convergent-beam patterns

A series of ten energy-filtered convergent-beam patterns was taken with the beam stepped by 10 nm between each pattern (giving a change in thickness of 20 nm). The beam diameter was about 1 nm; as a result each pattern is averaged over a thickness range of about 2 nm. Two convergent-beam patterns from the series are shown in Fig. 1 along with images simulated using the EMS Bloch wave program cb2 for corresponding specimen thicknesses. For the simulations, Debye–Waller factors of 0.0062 nm^2 for Ga and 0.0049 nm^2 for As [16] and an absorption of $V_0' / V_0 = V_g' / V_g = 0.05$ were used. The absorption value was chosen to match the rate of decay of the total energy-filtered intensity of the convergent-beam patterns with thickness, and it also matches the decay of the intensity of the lattice images well. It can be seen that the experimental and simulated convergent-beam patterns match well for both thick and thin specimens, as expected from other convergent-beam studies [5–7]. This means that the amplitudes and phase of the scattered beams are being calculated correctly.

Figure 2 shows a graph of the intensities of the diffracted beams and the diffuse scattering as a function of thickness measured from the experimental convergent-beam patterns and plotted on an absolute scale where the incident beam intensity is 1. The diffuse scattering was estimated by measur-

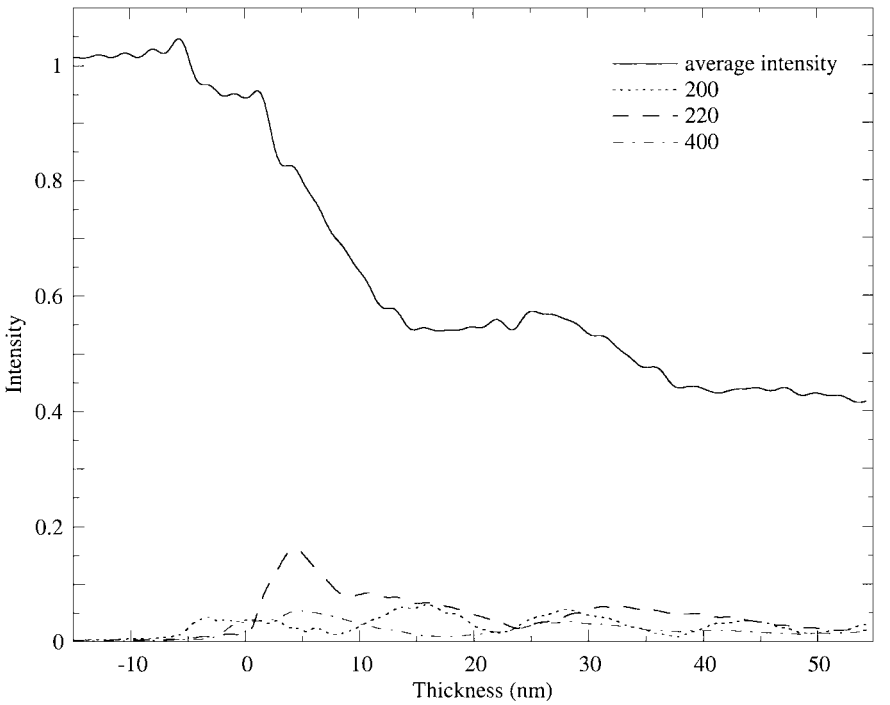

Fig. 4 Average intensity and amplitudes of lattice fringes measured from an experimental [001] GaAs lattice image with a defocus of –48 nm. The lattice fringe amplitudes for 200, 220, and 400 are the average of the 4 equivalent beams (opposite beams being necessarily equal). As for Fig. 2, negative thicknesses correspond to distances away from the edge of the crystalline part of the specimen into the contamination layer and all intensities are normalized so that the incident intensity is 1.

ing the diffuse intensity between the convergent-beam discs and extrapolating under the discs. The 000 and diffracted beam intensity was taken to be the sum of all the intensity in each convergent-beam disc after the diffuse intensity was subtracted. For the 200, 220, and 400 beams, the sum of all 4 equivalent beams is plotted. The thickness scale corresponds to the crystal thickness, which for a 90° wedge can be determined absolutely and confirmed by matching the convergent-beam patterns with simulations over all thicknesses. Negative thicknesses correspond to distances away from the edge of the crystalline part of the specimen into the carbon contamination. The diffraction pattern whose values are plotted at 0 nm crystal thickness was collected from just at the edge of the GaAs and, thus, corresponds to the diffraction pattern from amorphous carbon contamination only. Some contamination formed during the exposures and this was evident from comparing bright-field images before and after the convergent-beam patterns were taken. It can be seen from the values at 0 nm in Fig. 2 that 25% of the electrons are lost from the filtered convergent-beam pattern (i.e. scattered to high angles or inelastically), and 12% are scattered diffusely leaving only about 60% in the 000 beam. For thicker GaAs, some increase in the diffuse scattering is seen before this decreases as electrons are lost to inelastic and high angle scattering.

Figure 2 should be compared with the similar graph shown in Fig. 3 for convergent-beam patterns simulated for thickness steps of 5 nm. In the simulations there is no diffuse scattering present between the GaAs diffracted beams as the Debye–Waller factor was used to model phonon scattering. Although the thickness fringes are less evident in the experimental graph (Fig. 2) than in Fig. 3 due to the coarseness of the thickness steps between the experimental convergent-beam patterns (20 nm), it can be seen that, if diffuse scattering is ignored, the intensities of each beam relative to the total diffracted beam intensity match well. This is to be expected at the high thicknesses used for previous convergent-beam matching experiments. It is important to note, however, that the good match holds for all thicknesses down to the lowest, 25 nm. This confirms that simulations do predict the beam intensities well even for low thicknesses and that incorrectly calculated beam intensities are not the cause of the mismatch between experimental and simulated lattice images.

Returning to the diffuse scattering, as a proportion this increases from ~16% of the total scattering at 0 nm thickness (contamination) to 33% at 25 nm and 43% at 45 nm. To a good approximation, this diffuse intensity will produce no contrast in the corresponding lattice image (other than amorphous speckle) and it therefore just adds a constant background intensity to lattice images. A thickness of 25 nm is fairly thick for a lattice image, but even at this thickness the 33% diffuse scattering would only reduce the lattice fringe contrast to 2 / 3 of its original value. This is, in any case, an overestimate of the diffuse scattering as there was more contamination on the GaAs after collecting the convergent beam patterns than after the lattice images.

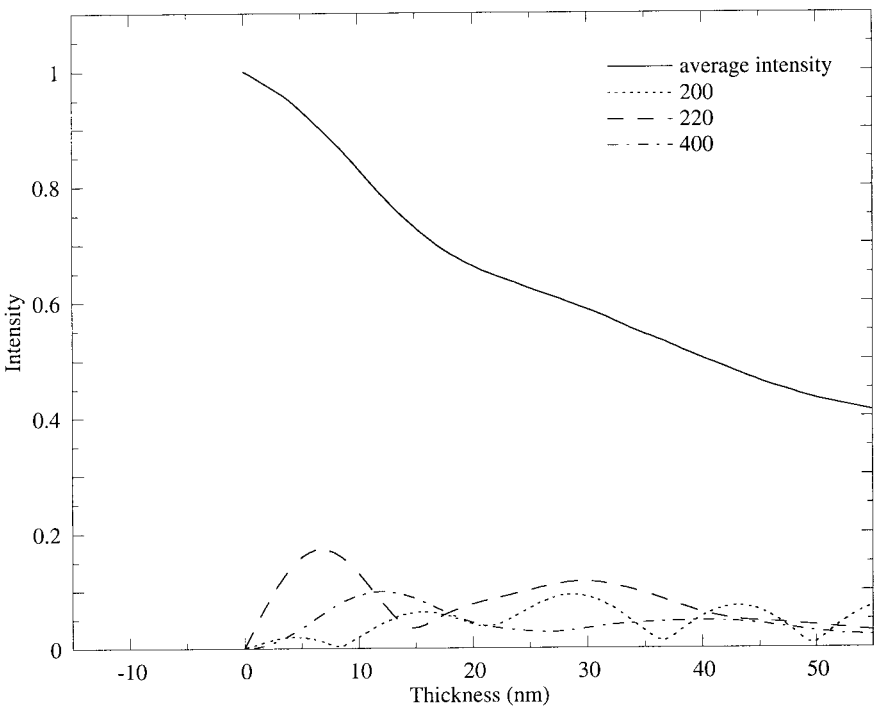

Fig. 5 Average intensity and amplitudes of lattice fringes measured from simulated [001] GaAs lattice images and plotted in a similar way to Fig. 4.

Lattice images

Lattice images were collected from an uncontaminated region adjacent to the convergent-beam patterns using an objective aperture of radius 26.4 mrad (13.3 nm^{-1}, i.e. just excluding the 800 beams) to give a well defined limit to the scattering angle. In the subsequent analysis, a lattice image with a defocus of –48 nm, near to the Scherzer defocus of –48.8 nm for the CM300, was analysed. To determine the lattice fringe amplitudes, the Fourier transform of this image was calculated. For each beam, an aperture of radius 1.77 nm^{-1} ($\frac{1}{4}g_{200}$) was drawn centred on the beam and everything outside this aperture in the Fourier transform set to zero. The centre of the Fourier transform was moved to coincide with the centre of the beam and a back-transformation performed. This produces a map of the amplitude of the set of lattice fringes corresponding to the beam, and for simplicity the 200 and 020, 220 and $\bar{2}20$, and 400 and 040 fringe amplitude maps were averaged together. From each of these maps, a 140.0 by 6.6 nm wide strip was cut with the long axis of the strip oriented along the direction of increasing crystal thickness and positioned to include areas from beyond the edge of the contamination layer to a crystal thickness of 55 nm. This strip was then averaged along its short direction, i.e. parallel to the edge of the GaAs crystal, with no averaging performed in the direction of increasing crystal thickness. The resulting intensity is plotted in Fig. 4 as a function of specimen thickness on an absolute scale. Again, negative thicknesses refer to distances away from the edge of the crystalline part of the specimen towards the vacuum and there is about 5 nm of contamination. In the contamination layer at 0 nm crystal thickness the average intensity drops to 95%, which can be compared to a drop to 75% for the similar measurement from the convergent-beam patterns, showing that there is less contamination on the lattice images.

Figure 4 should be compared with the lattice fringe amplitudes from simulated images shown in Fig. 5. The lattice images were calculated for thickness steps of 0.565 nm using a multislice program within Semper. The same parameters as used for the convergent-beam simulations in Fig. 3 were used, except that a crystal tilt of 2.4 mrad, corresponding to that measured after the lattice images were taken, was used. Although the crystal tilt was accidental, it was also fortuitous as this made the calculation less dynamical and, thus, less sensitive to the exact crystal tilt. For the image part of the calculation, a focal spread of 5 nm and a beam convergence of 0.6 mrad were used. Both of these are overestimates and no larger values could have been used, as they would have reduced the 220 and 400 fringe amplitudes too much relative to the 200 fringe amplitude. A similar Fourier process to that described for the experimental lattice images was used to determine the lattice fringe amplitudes, except that each simulated lattice image thickness was processed separately.

It can be seen by comparing Figs 4 and 5 that qualitatively

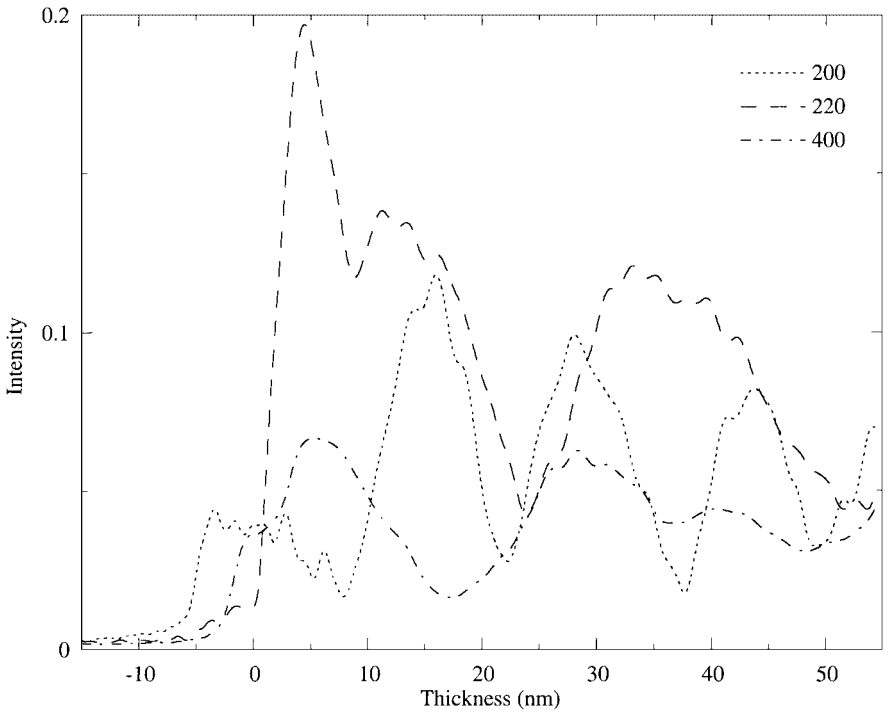

Fig. 6 Experimental lattice fringe amplitudes from Fig. 4 divided by the average intensity (solid line in Fig. 4).

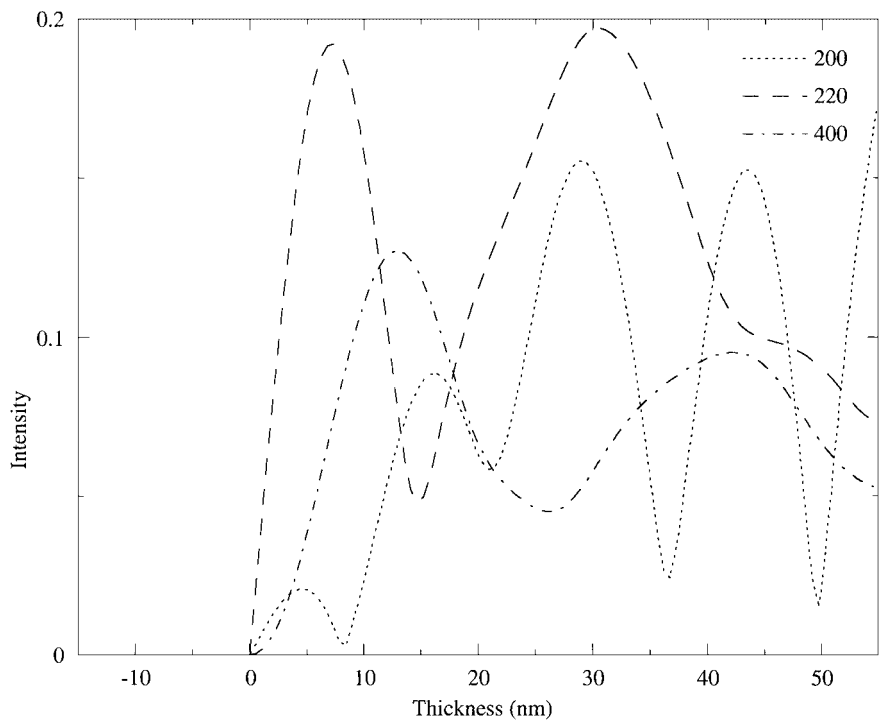

Fig. 7 Simulated lattice fringe amplitudes from Fig. 5 divided by the average intensity (solid line in Fig. 5).

both the variation of the fringe amplitudes with thickness matches and the average intensity decays at the same rate, meaning that the correct value of V_0' was used. The 220 fringe amplitude rises rapidly to a maximum at about 5 nm and has a second maximum at around 30 nm thick, while the positions of the minima and maxima of the 200 and 400 fringe amplitudes agree well. What is also evident from Figs 4 and 5 is that the experimental fringe amplitudes are lower than the simulations. This can be seen more clearly when the relative fringe amplitudes are calculated by dividing by the average intensity,

as shown in Figs 6 and 7.

Comparing Figs 6 and 7, we can see that up to 5 nm thickness there is a good match between the experimental and simulated fringe amplitudes. Both are dominated by 220 fringes and their amplitudes are comparable. However, for thicknesses between 5 and 20 nm the discrepancy becomes more apparent and above 20 nm thick the experimental fringe amplitudes are about half of the simulated amplitudes. This ratio varies with thickness and between each beam and this is about the best that can be expected from matching one defocus. A better match would require a focal series with each defocus determined accurately and the aberrations (e.g. coma and 3-fold astigmatism) determined accurately from a tilt series. However, errors in the measurement of the lens aberrations will not alter the overall conclusion that above about 20 nm thickness, the experimental fringe intensities are half the simulated intensities. If the estimate of the beam convergence is wrong or specimen drift or vibration were causing the low experimental contrast, then the fringe amplitudes would be reduced over all thicknesses, not just above 20 nm.

Concluding remarks

It has been shown that the details of convergent-beam patterns and their beam intensities match simulations well at both low and high thicknesses, but only when the diffuse background intensity is subtracted from the experimental patterns. Lattice image fringe amplitudes are comparable for the lowest 5 nm thickness but above 20 nm thickness are about half those from simulations. This is in approximate agreement with the factor of three discrepancy found for amorphous carbon [11] and a factor of three reduction in the measured phase of KI in nanotubes [17].

Measurements from convergent-beam patterns show that, for 25 nm thick GaAs, 33% of the electrons are diffusely scattered, rising to 43% at 45 nm thick. To cause the observed low lattice fringe amplitude at a thickness of 25 nm, 50% of the electrons would have to be diffusely scattered, not 33% as measured from the convergent-beam patterns. Thus, diffuse scattering from phonons and amorphous carbon are not the sole causes of the observed low lattice fringe contrast, although the decrease of lattice fringe contrast with thickness in line with the increase in diffuse scattering does suggest that diffuse scattering is part of the problem.

There was more contamination on the diffraction patterns than on the lattice images. This means that the diffuse scattering measured from the convergent-beam patterns is an overestimate of the diffuse scattering contributing to the lattice images, further emphasizing the point that diffuse scattering alone is insufficient to explain the low lattice fringe contrast.

The values of focal spread and convergence used to simulate the lattice images, whilst being comparable with those used elsewhere for field emission microscopes [17], are in reality an overestimate. More realistic values would be 2 nm instead of 5 nm for the focal spread and 0.2 mrad instead of 0.6 mrad for the beam convergence. These values would make the fringe contrast in the lattice images much greater and, thus, increase the discrepancy with the experimental lattice images.

Measurements of the lattice fringe contrast in annealed sapphire that had no surface contamination or other amorphous layers showed good agreement with simulations [18]. This, perhaps, suggests that amorphous surface layers are important in reducing contrast. On the other hand, if surface layers were so important, I would expect to find the lowest lattice fringe contrast at the lowest thicknesses, in fact the reverse was true. It does show that it is important to repeat this work with clean contamination-free specimens.

An important point to consider is the shape of the phonon scattering distribution in the diffraction pattern around the diffraction maxima. In this work it was assumed that this distribution was uniform as in the Einstein model, whereas a more realistic Debye model predicts phonon scattering to be peaked at the diffraction maxima. It is important that the extent of this approximation is determined in future work.

Acknowledgements

I would like to thank R. Dunin-Borkowski for useful discussions.

References

1 Hÿtch M J and Stobbs W M (1994) Quantitative comparison of high resolution TEM images with image simulations. *Ultramicroscopy* **53**: 191–203.

2 Boothroyd C B, Dunin-Borkowski R E, Stobbs W M, and Humphreys C J (1995) Quantifying the effects of amorphous layers on image contrast using energy filtered transmission electron microscopy. In: *MRS Symposium Proceedings*, Vol. 354, eds Jacobson D C, Luzzi D E, Heinz T F, and Iwaki M, pp. 495–500, (MRS, Pittsburgh).

3 von Hochmeister K and Phillipp F (1998) Quantitative comparison of HREM images with image simulations. In: *Electron Microscopy 96*, Vol. 1, ed. Committee of European Societies of Microscopy, pp. 418–419, (Committee of European Societies of Microscopy, Brussels).

4 Boothroyd C B (1997) Why don't high resolution simulations and images match? *J. Microsc.* **190**: 99–108.

5 Zuo J M and Spence J C H (1991) Automated structure factor refinement from convergent-beam patterns. *Ultramicroscopy* **35**: 185–196.

6 Bird D M and Saunders M (1992) Sensitivity and accuracy of CBED pattern-matching. *Ultramicroscopy* **45**: 241–251.

7 Midgley P A and Saunders M (1996) Quantitative electron diffraction: from atoms to bonds. *Contemp. Phys.* **37**: 441–456.

8 Watanabe H, Fukuhara A, and Kohra K (1962) Measurement of mean and anomalous absorption coefficients of electrons in MgO crystals by the use of electron micrographic images. *J. Phys. Soc.* **17**: 195–199.

9 Metherell A J F (1967) Measurement of absorption of fast electrons in single crystal films of aluminium. *Philos. Mag.* **15**: 755–762.

10 Dunin-Borkowski R E, Schäublin R E, Walther T, Boothroyd C B, Preston A R, and Stobbs W M (1995) The determination of absorption parameters in Si and GaAs using energy filtered imaging. In: *Electron Microscopy and Analysis 1995*, Vol. 147, ed. Cherns D, pp. 179–182, (Institute of Physics Publishing, Bristol).

11 Boothroyd C B (2000) Quantification of high-resolution electron microscope images of amorphous carbon. *Ultramicroscopy* **83**: 159–168.

12 Loane F, Xu P, and Silcox J (1991) Thermal vibrations in convergent-beam electron diffraction. *Acta Cryst.* **A47**: 267–278.

13 Rez P, Humphreys C J, and Whelan M J (1977) The distribution of intensity in electron diffraction patterns due to phonon scattering. *Phil. Mag.* **35**: 81–96.

14 Bursill L A and Rossouw C J (1984) Dynamical excitation of thermal diffuse scattering in crystals of rutile. *J. Microsc.* **136**: 153–163.

15 Wang Z L (1992) Dynamics of thermal diffuse scattering in high-energy electron diffraction and imaging: theory and experiments. *Phil. Mag. B* **65**: 559–587.

16 Saravanan R, Mohanlal S K, and Chandrasekaran K S (1992) Anharmonic temperature factors, anomalous dispersion effects and bonding charges in gallium arsenide. *Acta Cryst.* **A48**: 4–9.

17 Meyer R R, Sloan J, Dunin-Borkowski R E, Kirkland A I, Novotny M, Bailey S R, Hutchison J L, and Green M L H (2000) Discrete atom imaging of one dimensional crystals formed within single walled carbon nanotubes. *Science* **289**: 1324–1326.

18 Lloyd S J, Dunin-Borkowski R E, and Boothroyd C B (1997) The determination of the ionicity of sapphire using energy-filtered high resolution electron microscopy. In: *Electron Microscopy and Analysis 1997*, *Inst. Phys. Conf. Ser.*, No. 153, ed. Rodenburg J M, pp. 113–116, (IOPP, Bristol).